batteries

MDPI

Article

Adaptive Transfer Learning Strategy for Predicting Battery Aging in Electric Vehicles

Daniela Galatro [1], Manav Shroff [1] and Cristina H. Amon [1,2,*]

[1] Department of Chemical Engineering and Applied Chemistry, University of Toronto, Toronto, ON M5S 3E5, Canada; daniela.galatro@utoronto.ca (D.G.); manav.shroff@mail.utoronto.ca (M.S.)
[2] Department of Mechanical and Industrial Engineering, University of Toronto, Toronto, ON M5S 3G8, Canada
* Correspondence: cristina.amon@utoronto.ca

Abstract: This work presents an adaptive transfer learning approach for predicting the aging of lithium-ion batteries (LiBs) in electric vehicles using capacity fade as the metric for the battery state of health. The proposed approach includes a similarity-based and adaptive strategy in which selected data from an original dataset are transferred to a clean dataset based on the combined/weighted similarity contribution of feature and stress factor similarities and times series similarities. Transfer learning (TL) is then performed by pre-training a model with clean data, with frozen weights and biases to the hidden layer. At the same time, weights and biases toward the output node are recalculated with the target data. The error reduction lies between −0.4% and −8.3% for 20 computational experiments, attesting to the effectiveness and robustness of our adaptive TL approach. Considerations for data structure and representation learning are presented, as well as a workflow to enhance the application of transfer learning for predicting aging in LiBs.

Keywords: adaptive transfer learning; electric vehicle; battery aging; time series similarities

Academic Editor: Pascal Venet

Received: 2 December 2024
Revised: 2 January 2025
Accepted: 6 January 2025
Published: 9 January 2025

Citation: Galatro, D.; Shroff, M.; Amon, C.H. Adaptive Transfer Learning Strategy for Predicting Battery Aging in Electric Vehicles. *Batteries* **2025**, *11*, 21. https://doi.org/10.3390/batteries11010021

1. Introduction

Aging in lithium-ion batteries (LiBs) describes the gradual decline of their performance over time. This deterioration is caused by side reactions to the primary ion-intercalation reaction, such as the formation and growth of the solid electrolyte interface (SEI) and lithium plating, as well as electrode degradation, electrolyte decomposition, and mechanical stress [1]. The battery's overall condition compared to its initial state is known as its state of health (SOH). Capacity is typically used as a metric for the SOH, decreasing as the battery ages. Capacity fade is influenced by several stress factors, such as temperature, state-of-charge (SOC), depth-of-discharge (DOD), and charge/discharge rates (C-rate). Thus, high temperatures (>45 °C) are conducive to increasing the SEI thickness at the anode surface, creating internal resistance that reduces capacity and increases mechanical stress on the anode [1]. Low temperatures (<10 °C), on the other hand, cause lithium plating (LP), where lithium deposits on the anode surface during charging. Moreover, LP is also caused by high charge rates, since lithium ions quickly intercalate into the anode, leading to plating. Both SEI growth and LP cause capacity loss, as lithium is unavailable for intercalation. LP is also known to increase the risk of thermal runaways [1]. Aging affects the performance, safety, and cost-effectiveness of electric vehicles (EVs) over time, as the battery is the most critical part of the vehicle, driving the lifespan and use of EVs. The choice of the electrolyte impacts the aging process of LiBs [2] since (i) different electrolytes affect the stability and uniformity of the SEI, (ii) some electrolytes are prone to produce byproducts as they decompose, reducing the battery capacity over time, (iii) lithium deposits leading to

plating may also vary depending on the selected electrolyte, and (iv) certain electrolytes not suited for specific operating conditions can lead to mechanical stress and battery physical degradation.

Several approaches have been used to model aging in LiBs, including empirical, electrochemical, and data-driven models. Empirical models, mostly in the shape of equivalent circuit models (ECMs), have been used to represent the dynamic behavior of the battery [3,4]. ECMs are simple, computationally efficient, and can be easily implemented in real-time applications [5,6]. Nevertheless, their accuracy can be compromised as they might not capture sensitive electrochemical processes occurring within the battery. Electrochemical models, on the other hand, can overcome this drawback, as they offer insights into these processes [1,5–7]. Their main disadvantages are their complexity and demanding computational time, as they require providing several parameters to describe the battery's materials and processes [6]. Data-driven models are adaptable and can identify complex patterns during real-time monitoring, as they are fundamentally supported by efficient techniques within the machine learning and/or deep learning domains [8–10]. The main drawbacks of these models are that they might lead to overfitting/underfitting (without proper validation), they can be computationally intensive, and might lack interpretability. The validation of data-driven models is mainly performed using lab-based testing employing cycling tests, accelerated aging tests (exposing cells to extreme temperature, C-rate, SOC, and/or DOD), and electrochemical impedance spectroscopy (EIS). While lab-based testing offers controllability and repeatability, they are resource-consuming and might be limited, as they might not replicate vast real-world usage scenarios [5,7]. The challenge can be framed as data availability, for which transfer learning (TL) can potentially be used to adapt models trained on datasets from one type of battery or operating condition and consequently predict aging in another battery with limited data. Transfer learning is known to be effective in improving generalization from limited data while potentially enhancing model performance [11].

Some considerations that must be taken when applying transfer learning include setting aspects such as feature overlaps, similarity of tasks, sufficient and/or distributed data, layer transferability and fine-tuning strategy, potential sources of overfitting, use of representative and accurate pre-trained models, and, finally, selecting proper validation techniques such as cross-validation, and/or error analysis [12]. Other specific aspects that must be considered when applying transfer learning include regimes of parameterization/test errors (under-, abundant, and superabundant) and learned representations [13,14]. Thus, (i) superabundant models are well suited for TL because they tend to find generalized solutions, (ii) test error regimes are useful to assess generalization, and (iii) combining abundant parameterization and hierarchical representation learning allows for capturing complex patterns. These insights [13,14] might be constrained by domain gap and domain adaptation, data noise, small target datasets, demanding computational resources when overparameterizing models or tuning hyperparameters, potential overfitting if models are not properly regularized, and non-monotonic test error (double or triple descend), as these models can exhibit complex error behaviors. These limitations can be addressed with adaptation, regularization, and alignment with the target domain [12]. In predicting capacity fade in LiB using TL, underparametrized models may fail to capture the complexity of degradation mechanisms using capacity fade only. Learned representations, on the other hand, affect transferability, for instance, using lower layers to capture general degradation patterns, such as capacity fade across different datasets.

A typical TL approach to predict SOH in LiBs would involve using a pre-trained model illustrating capacity fade time series at different operating conditions within a neural network architecture; the pre-training model is then tuned on the target domain data, and

layer freezing is performed by keeping the initial layers of the model frozen (as they capture general features) and only tuning the later features to capture specific features. Examples of TL applications for predicting battery aging features were presented by [15–17]. The authors in [15] propose a model to predict remaining useful life (RUL), which can be adapted to different battery types. In their approach, iterative transfer learning is used to transfer pre-trained models from a source domain to a target domain; Mogrifier Long Short-Term Memory was used to enhance input–output interactions by adding gating units, improving prediction accuracy and stability. While promising, this approach heavily relies on the quality and quantity of the source domain data. Moreover, generalization of the model to other battery chemistries can be a challenge, and model interpretability remains limited. In the work presented in [17], TL proved to accurately predict capacity and RUL while being robust across different datasets and operating conditions. Some potential drawbacks of this work include the use of limited data and lack of result interpretability. Nevertheless, as proven in other TL applications, beyond the experimental setup used to generate the data to fit/model, specific considerations over the bias–variance tradeoff must be taken (e.g., understanding the double descent/triple descent phenomenon), as this can help researchers guide decisions on model complexity and training strategies [13].

As the capacity fade over time is a time series, we propose an adaptive transfer learning approach to predict capacity as an aging metric by selecting the source data based on features/stress factors similarities (SFS) and time series similarities (STS), as this selection process can improve the effectiveness of TL for time series forecasting. Thus, similarity algorithms, such as Dynamic Time Warping (DTW), can measure the similarity between time series datasets by selecting datasets similar to the target data, allowing the pre-trained model to capture relevant patterns [18]. The total data similarity (TDS) is then introduced as a weighted function of SFS and STS through a contribution factor α, a fraction between 0 and 1 that denotes similarity for STS and SFS, and therefore, the contribution of features and time series to aging. Moreover, we also set an arbitrary similarity TDS threshold of β, which implies that those TS subsets or experiments with TDS less than or equal to β are transferred from the original to a clean dataset, which includes similar time series and features to the target data.

We hypothesize that this TL approach improves model accuracy and robustness while reducing computational time. We compiled aging data from the literature of 100 experiments reporting capacity fade over time for nickel manganese cobalt (NMC) oxide cells cycled at different operating conditions to illustrate a representative combination of stress factors during cycling that promote different aging trajectories. Moreover, some datasets include several cells cycled to the same operating conditions, allowing us to consider cell-to-cell variation (i.e., spreading). Our approach also serves as a framework for efficiently validating data-driven LiB aging models.

2. Methodology

Our transfer learning workflow, shown in Figure 1, starts by compiling or generating diverse LiB aging data, including different nominal capacities, cell chemistries, formats, operating conditions, and aging-related indicators, such as capacity, resistance, and voltage. Comprehensive test matrices intended to fairly capture battery aging mechanisms within an operational envelope are presented in [5].

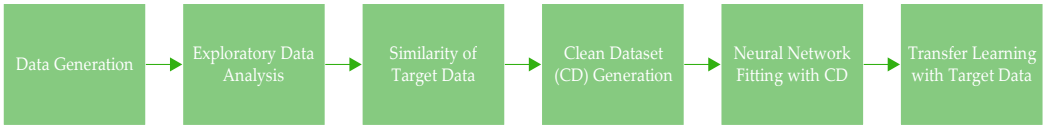

Figure 1. Transfer learning workflow.

2.1. Transfer Learning Workflow

Once compiled, we perform exploratory data analysis (EDA) on the compiled/generated data to identify patterns and account for outliers and missing values. EDA is followed by quantifying the similarity of the limited target data with the complete dataset, aiming to select the most similar source data to the target one and create a clean dataset (CD), which includes similar time series and features to the target data.

The neural network (NN) is then fitted with the CD, and the transfer learning is performed using freezing techniques. We then use error metrics for validation and comparison purposes.

2.2. Datasets

In this work, the original dataset (OD) is composed of 1000 data points extracted from figures and tables in the literature, representing 100 experiments reporting capacity fade over time for NMC cells from different nominal capacities, chemistry blending, and formats at different operating conditions.

While the experimental setup used to generate the data varies in terms of ranges/values of stress factors and number of cells tested across the investigated literature (as there are no standard protocols to test battery aging based on an explicit design of experiment), there are some important considerations to highlight regarding it:

- Most experiments gather capacity fade over time in cycling tests during the cell's first life (before reaching the first-life threshold at 80% of the initial capacity). Some high C-rates experiments allowed recording capacity fade values beyond the 80% threshold, capturing the nonlinear aging region due to lithium plating;
- Cycling tests include different SOC and DOC conditions, as well as low, medium, and high temperatures;
- Some cycling tests are performed at accelerated conditions (up to 60 °C or low temperatures promoting/accelerating plating, DODs of 80 and 100%, and high C-rates up to 6) to speed up the aging process;
- Some datasets report additional aging-related indicators such as voltage and internal resistance/impedance;
- Cell nominal capacity ranges from 0.088 to 64 Ah, including prismatic, pouch, and cylindrical formats, and 111, 433, 442, 532, 622, and 811 NMC chemistries, listed in Appendix A [19–48]. Data from experiments including two or more cells cycled at the same conditions were merged using a three-parameter non-homogeneous Gamma distribution to account for cell spreading [49,50];
- No post-mortem analyses on cells (e.g., scanning electron microscopy, X-ray diffraction, or nuclear magnetic resonance) were assessed.

Detailed information on the datasets we compiled is shown in Appendix A.

2.3. Similarity and Neural Network Architecture

The original dataset is transformed into a clean dataset by selecting the source data of the transfer learning process based on features/stress factors and time series similarities. Thus, the target data are compared against the 100 time series (one per experiment) of the original dataset, and the clean dataset is built based on the data experiments most similar to the target one. The criteria for determining similarity and generating a clean dataset are discussed later in this section. They include combining the Frobenius norm for features and stress factors and a similarity time series algorithm. The clean dataset is then used to build the corresponding neural network (NN) for transfer learning.

The input data can be clustered in two domains: features/stress factors and time. Features include the cell's nominal capacity, chemistry, and format, while stress factors

affecting aging are the temperature, average SOC, DOD, and C-rate. When we look at the capacity fade as a function of time per experiment, we are referring to a time series. Hence, each experiment is a time series.

Similarity for the features and stress factors is assessed within the clean dataset by looking at matrix A, composed of values of nominal capacity, chemistry, format, temperature, average SOC, DOD, and C-rate for each experiment, and comparing it against a matrix B, including the features and stress factors of the target data. In this work, we use the Frobenius norm to estimate the similarity between A and B by calculating the norm, which provides a single scalar value obtained by taking the square root of the sum of the absolute squares of their elements:

$$\|A - B\| = \sqrt{\sum_{i=1}^{m} \sum_{j=1}^{m} (a_{ij} - b_{ij})^2} \quad (1)$$

This difference represents the "distance" between matrices A and B, as per the Frobenius norm method. The smaller this value, the more similar these matrices are.

Similarity for the times series is assessed within the clean dataset by looking at capacity fade over time for each experiment and comparing it against the capacity fade of the target data. In this work, we use the Dynamic Time Warping (DTW) similarity algorithm, which effectively compares two temporal sequences that vary in "speed", as in the compiled data. DTW works by aligning the two-time series by warping the time axis to minimize the distance between them, either stretching or compressing them. A cost matrix is then created by populating the distance between each point in one time series and every point in the other time series. Finally, a warping or optimal path shows the best alignment between the time series. The corresponding DTW math is as follows:

Step 1: A distance matrix of elements between two series is calculated (Euclidean distance);

$$d(i,j) = \sqrt{(x_i - y_i)^2} \quad (2)$$

Step 2: An accumulated cost matrix D is constructed, where the minimum cost to align the time series is included;

$$D(i,j) = d(i,j) + min \begin{pmatrix} D(i-1,j) \\ D(i,j-1) \\ D(i-1,j-1) \end{pmatrix} \quad (3)$$

Step 3: The warping path defines the optimal alignment between X and Y by choosing the cost path at each step.

The DTW algorithm is constrained to three conditions: boundary, monotonicity, and continuity.

The similarity measure is the distance that shows the match between two sequences; hence, smaller distances suggest that the time series are more "alike". DTW does not require the same time step or time scale to compare time series.

In this work, total data similarity (TDS) is quantified by weights assigned to similarity for the time series (STS), and similarity for the features and stress factors (SFS), using the following aggregated equation:

$$TDS = \alpha STS + (1 - \alpha) SFS \quad (4)$$

where α is the contribution factor to TDS for STS and SFS, as a fraction between 0 and 1. TDS can be seen as a similarity index.

The value of α is iteratively obtained by minimizing the TL-SSE (sum of squares error) or calculated error between actual and predicted values after applying TL. STS, SFS, and TDS are normalized versions of their originally calculated values. We arbitrarily normalize these values to a range between 0 and 1 and set an arbitrary similarity TDS threshold of β. This implies that those TS subsets or experiments with TDS less than or equal to β are transferred from the original to the clean dataset, as smaller distances suggest that the selected TSs are more "alike" to the target data. Similarity is, therefore, defined by the contribution factor α and threshold value β (data corresponding to TDS $\leq \beta$), whose tuning process makes the proposed TL approach adaptative, with the source data adaptively selected for optimal knowledge learning and transfer.

The normalization of STS and SFS, before the linear combination presented in Equation (4), is performed by applying the following formulas:

$$STS = \frac{1}{1 + DTW(X, Y)} \tag{5}$$

$$SFS = \frac{1}{1 + \|X' - Y'\|_F} \tag{6}$$

Frobenius norm and DTW address similarity in different ways, as DTW focuses on alignment between time series, while Frobenius norm measures magnitude. By combining them, we can verify the alignment/time shifts in the time series while measuring the overall magnitude of the difference between the two time series based on the features. Overlap in "similarity extraction" can occur in some scenarios, for instance, when using the Frobenius norm after DTW alignment. A possible solution to avoid this overlap could be using DTW for time alignment first and then using the Frobenius norm to quantify the magnitude of the difference between the aligned series. In this work, we use the combined contributions from DTW and the Frobenius norm to form an aggregate or composite similarity score using a linear combination (weighted sum). Alternatively, multiplicative combination and maximization of the two similarities can also be used. To ensure that this combination does not result in overlapping similarities, we employ normalization of both metrics to ensure that each metric contributes to the similarity score in a balanced way. Ultimately, tuning α is an empirical task in combination with cross-validation.

The NN for TL is then fitted with the clean dataset. The NN architecture includes one input layer with the following features and stress factors: nominal capacity, chemistry, format, time, temperature, mean SOC, DOD, C-rate charge, and C-rate discharge. We chose one layer of hidden nodes since the capacity fade data are weakly nonlinear; a single hidden layer with an activation function such as hyperbolic tangent (tanh) can effectively predict the output, as noncomplex patterns are expected because of the capacity behavior of the experiments. Our NN architecture has one output layer with one variable, capacity, which fades or decreases over time per experiment. The optimal number of hidden nodes in the hidden layer is obtained by increasing its value from 10 until reaching an arbitrary sum of squared error (SSE) less than 1. The learning rate is also iteratively tuned, while regularization and early stopping are employed to prevent overfitting. Figure 2 illustrates the NN/TL architecture employed in this work. To our knowledge, no pre-trained datasets tailored to this application can be currently found in the literature.

As shown in Figure 2, six input nodes corresponding to the features/stress factors and time are linked through dashed blue lines to the hidden layer. A gray rectangle frames the input and hidden nodes, where frozen weights and biases from the input layer to the hidden layer lie. The red solid lines from the hidden layer to the output layer (capacity) represent the weights and biases to be modified/updated via optimization with the dataset from the task.

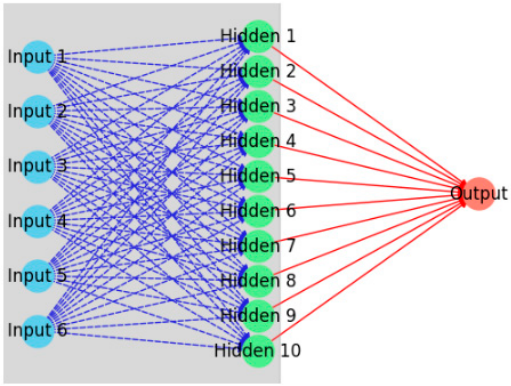

Figure 2. Transfer learning architecture.

Training–validation–testing sets to build the NN follow a 75%–15%–15% split, for a total of 1000 data points reduced to clean datasets including a number of data points depending on the similarities to the target data. Data leakage from training to validation and testing sets is avoided by selecting complete time series (for temporal leakage) or time-based splitting.

2.4. Transfer Learning

Once the architecture/structure of the NN is determined, the TL process is performed by replacing the weights and bias toward the response variable (capacity) with optimized values obtained by minimizing the root mean squared error (RMSE) between the predicted and actual response values. This process allows the hidden nodes to capture the relationship of the variables while enhancing the fitting for the limited data toward the output NN layer. Hence, the weights and bias of the last layer are recalculated using the data from the pre-trained model and the limited dataset from the task to minimize the error between the predicted $(\hat{y}_i)$ and actual outcome (y_i) for the combined dataset [11]. Therefore, pre-trained weights are shared for the new task, acting as a starting point for fine-tuning. The optimization is performed using the gradient-based Broyden–Fletcher–Goldfarb–Shann (BFGS) algorithm [11]. The BFGS algorithm is a quasi-Newton (gradient) based method that minimizes computational costs and exhibits fast convergence.

2.5. Validation and Comparison

Our adaptive TL approach is validated by randomly selecting experiments, extracting their corresponding time series data from the original dataset, and performing the transfer learning task as per our similarity-based approach to the source data. We then compare the predicted values of capacity for the limited dataset against the actual values, using the RMSE as a measure of discrepancy between these values.

3. Results and Discussion

In this section, we report the results of applying our adaptive TL approach to several sets of limited target data extracted from the original dataset.

The NN fitted with the original dataset reached an SSE of less than 1 when including 100 nodes in the hidden layer. This NN is named the original NN. We use experiments 5, 6, and 7 of the original dataset (Appendix A) to illustrate the implementation of our TL approach. These experiments studied the effect of charging rates on NMC 622 graphite pouch cells subjected to 30 °C, 50% SOC, and 100% DOD. Figure 3 shows the charging rate effect on the capacity fade for three C-rates of 1C, 4C, and 6C.

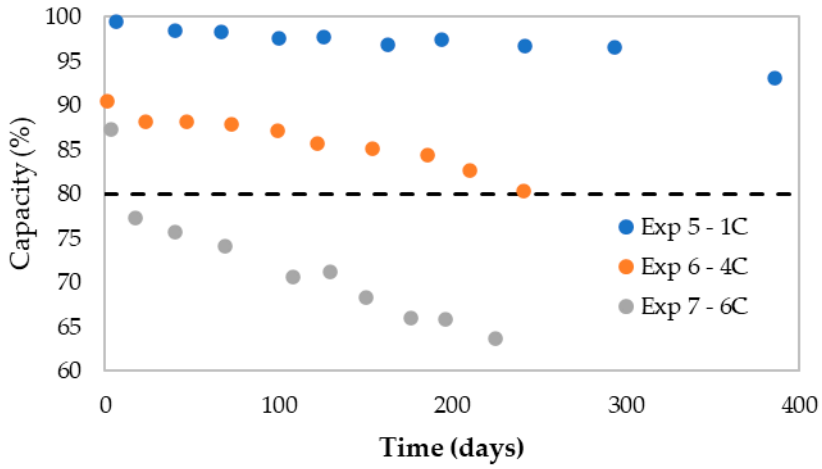

Figure 3. Effect of charging rates on capacity fade for experiments 5, 6, and 7 [22].

High charging rates accelerate the LiB degradation (i.e., aging), reducing their performance and, consequently, their lifespan, as shown in Figure 3. The first-life threshold of 80% capacity (horizontal line) is reached at 240 days for 4C and 10 days for 6C, considerably more aggressive than when charging at 1C, where cells do not reach this threshold until over 400 days, which is the maximum recorded time for the experiment.

In this example, the data for 1C and 4C (experiments 5 and 6) were removed from the original dataset. We defined six cases to illustrate the effect of α and β on the effectiveness of our TL approach, combining α = 0.2, 0.5, and 0.7, with β = 2.5 and 5. The TDS for each data point was calculated, and one clean dataset per case was created based on the threshold β. The NN architecture per case used for TL included an optimal number of hidden nodes in the hidden layer (obtained when SSE < 1) and was fitted with its corresponding clean dataset. Once fitted, the outlet weights and bias of each NN were refitted with the 6C data as target data. We then conducted the TL test on data that included 1C, 4C, and 6C. The error reduction between the TL without and with implementing similarity was reported as the accuracy metric of our approach.

When conducting experiments for modeling purposes in real life, experiments at 6C should be selected over 1C and 4C experiments, particularly when resources are constrained. The combination of stress factors, led by the high C-rate, accelerates the experiments, allowing capacity fade data to be obtained quickly. Hence, this example shows an application that might lead to a reduction in physical experiments, as TL could effectively predict capacity fade at the less aggressive combination of stress factors.

Table 1 shows the results of implementing our TL approach for this example, summarizing its performance across various configurations of α and β, evaluating the error reduction percentages for experiments 5, 6, and 7. Each configuration explores how the weighting of features/stress factors (α) and the threshold for similarity (β) affects the size of the clean dataset and transfer learning performance. The results provide insights into the tradeoffs between data structure, representation learning, and transfer learning effectiveness.

Each combination of α and β leads to different data points to be transferred from OD to CD, in which TDS values shall be less than or equal to β. The error reduction shows the percentage reduction, if any, when estimating the capacity of the target dataset without and with our TL approach. Positive error reduction values reflect a detriment in predicting capacity fade when using TL.

Table 1. Accuracy of the proposed transfer learning approach for different values of α and β for experiments 5, 6, and 7, with a number of hidden nodes in NN = 10 for all cases.

Case	α	β	Number of Data Points in Clean Dataset	Error Reduction, % [1]
1	0.2	0.25	100	Not calculated [2]
2	0.2	0.5	670	−1.2
3	0.5	0.25	270	>0
4	0.5	0.5	780	−3.5
5	0.7	0.25	390	−1.2
6	0.7	0.5	930	−4.7

[1] Error reduction implies improvement in accuracy (from the RMSE). [2] The resulting clean dataset only includes one cell SOC, for which its normalization fails.

Table 1 reveals that the best percentage reduction when estimating capacity fade for the target dataset corresponds to case 6 (α = 0.7 and β = 0.5), with a value of −4.7%, emphasizing the importance of features and stress factors over time series similarities when selecting the clean dataset to be used for transfer learning. This can be confirmed when looking at case 5, in which 70% of the similarity contribution (α = 0.7) is due to features and stress factors, leading to a CD of 390 data points for a threshold of β = 0.25. This means that transfer learning is effective in predicting capacity fade for limited data with only 40% of the original data points, contributing to a −1.2% error reduction. Conversely, case 2 shows that 67% of the original data points are required to reach the same error reduction if only 20% of the similarity contribution is due to features and stress factors.

Case 1 (α = 0.2 and β = 0.25), on the other hand, highlights the importance of having representative diverse data for effectively performing transfer learning. The calculated number of data points for this case is 100, compared with the original dataset that includes 1000 data points. The error reduction cannot be calculated, as the resulting CD only includes one cell SOC (50%), for which its normalization fails. Case 3 reports a reduction error greater than zero, showing no improvement after applying transfer learning, suggesting that the trade-off similarity/diversity and representativity of the data were not effective for the process. These observations are aligned with data representation, data invariance, and fundamental settings applied to transfer learning [12].

Some key takeaways from Table 1 are summarized as follows:

- The results highlight the critical role of representation learning in transfer learning. Thus, configurations with higher α values (e.g., cases 5 and 6), which emphasize the contribution of features/stress factors, tend to outperform those relying on time series similarity (e.g., cases 1 and 2). This finding aligns with the data invariance and representation learning principles, where capturing meaningful and transferable features enhances the adaptation to the target domain;
- The threshold β is crucial in determining the clean dataset size. Higher thresholds (e.g., $\beta = 0.5$) lead to diversity and improved model generalization (like in case 6), while restrictive or low thresholds (e.g., $\beta = 0.25$) decrease the dataset's representativity, negatively impacting the TL performance (as seen in Cases 1, 3, and 5). These results highlight the importance of balancing similarity and diversity when selecting data for transfer learning to ensure relevance and representation of the target domain;
- Larger clean datasets typically correlate with better TL performance metrics. Nevertheless, it has been proven that including representative and diverse data is as important as its size.

Some recommendations derived from this analysis include the following:

- Feature/stress factors shall be prioritized over time series similarities when selecting data for TL, as these are more transferable across domains;

- β thresholds shall be moderate to ensure a balance between diversity and relevance to the target task. Thus, over-restricted thresholds shall be avoided, as they might result in unrepresented datasets, leading to failure in normalization and transferring.

The implementation of similarity contribution factors or weights could be improved using feature importance techniques, as these techniques could potentially support obtaining a strong correlation with the target data. Overfitting and/or not capturing the complexity of the data might also be expected if not treated/implemented properly. The use of Random Forest in this work did not prove any significant improvement, as this technique does not rely on distance or similarity.

While the calculated error reductions for all cases and computational experiments seem relatively low, the error reduction range is significant (approximately −8.3% in RMSE). Errors ultimately depend on the nature of the aging data, including its diversity within an operational envelope, complex patterns associated with nonlinear behavior, and cell chemistry, among other factors. Moreover, these errors might vary among other aging indicators.

Another significant consideration for transfer learning is the diversity in the target data. In experiments 5, 6, and 7, the data only vary in time, capacity, and C-rate, as our goal is to evaluate the effect of C-rate on aging. When preparing the target data for TL, we randomly added +16% of data points from the original dataset minus data from experiments 5, 6, and 7, making sure that the code reads diverse values in all features and stress factors so the target data can be properly normalized. The total number of data points in the target dataset is 36.

The previous findings led us to test the original dataset, excluding experiments 5 and 6, to predict the capacity fade for 1C and 4C without employing any TL approach. Transfer learning reduces the error by −0.6% and −0.9% for TL without and with similarities (α = 0.7 and β = 5), respectively, when compared to predictions from an NN of 80 hidden layers.

The computational time between the transfer learning process without and with applying similarity decreases from an average of 1 h 46 min to 1 h 24 min when running Case 6 with the software R 4.1.1 in a 2.60 GHz processor with 32 GB memory RAM. R is a software and programming language widely used in data analysis, including time series analyses.

Table 2 compares neural network performances for the original and clean datasets, against transfer learning. As shown in Table 2, transfer learning outperforms the neural network models from the original and clean datasets in terms of prediction accuracy, exhibiting lower RMSE, and model fit, showing higher R^2, demonstrating its effectiveness. The average error reduction for experiments 5, 6, and 7, from the original dataset NN to transfer learning, is −4.9%.

Table 2. Comparison between neural network performance for the original and clean datasets against transfer learning (case 6).

Experiment	Original Dataset		Clean Dataset		Transfer Learning		Error Reduction, %
	RMSE	R^2	RMSE	R^2	RMSE	R^2	
5	8.2	0.77	7.4	0.81	3.2	0.93	−5.0
6	9.3	0.72	8.6	0.79	4.2	0.90	−5.1
7	8.7	0.75	8.2	0.80	4.0	0.92	−4.7
Average	8.7		8.1		3.8		−4.9

Note: R^2 is the coefficient of determination.

Figure 4 summarizes the results of applying our adaptive TL approach for a representative set of 20 computational experiments for optimal values of α and β within the original dataset. The error reduction lies between -0.4% and -8.3% for 20 computational experiments. The source data for each computational experiment were adaptively selected for optimal knowledge learning and transfer by tuning the contribution factor α and the threshold value β.

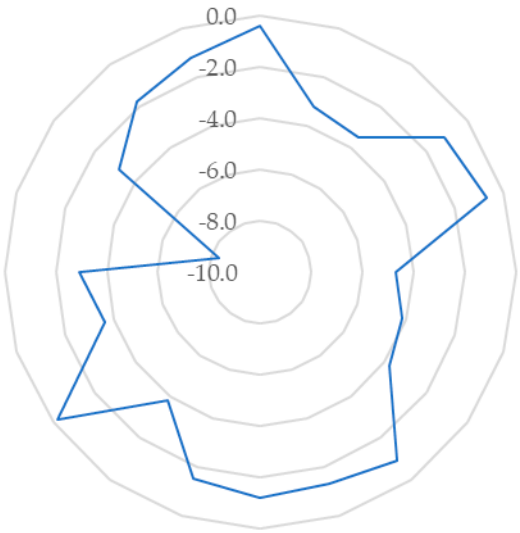

Figure 4. Error percentage reduction for 20 computational experiments for optimal values of α and β and number of hidden nodes (NH) = 10.

The NN architecture and its corresponding tuning strategies, specifically defining the number of hidden nodes, learning rate, and convergence criteria, play a crucial role in transfer learning. Thus, early/middle layers are frozen to keep the main NN features and capture patterns, and the final layer weights and biases are refitted or tuned to tailor the pre-trained model to the new task of predicting capacity fade for the target data. Hence, accurate pre-trained models are prerequisites for transfer learning in terms of better performance on the target task and might explain, in addition to the nature of the data itself, the relatively low estimated error reductions.

Previously, we emphasized that the optimal number of hidden nodes (NH) in the hidden layer was the main parameter modified when obtaining the pre-trained model for TL. The progression/decrement of the SSE from an arbitrary value of NH = 10 to the optimal number of nodes, obtained when reaching an arbitrary SSE less than 1, allowed us to frame the optimal number between 5 and 15 for all original and clean datasets.

While our TL approach was applied to capacity fade as an aging indicator, this proof-of-concept exercise could be extended by adding other aging variables of interest, such as impedance and voltage, and hence, gaining a better insight into the battery SOH.

Further analysis shall be conducted to study the trade-off between similarity, data diversity for normalization, and the consequent number of points to be transferred to the CD, as this affects the accuracy of the TL approach. Intrinsic limitations are associated with finding optimal combinations of α and β as this might lead to increasing computational time.

Regarding the similarity algorithms, as the Frobenius norm of the difference between two matrices requires them to be both of size $m \times n$, other similarity algorithms shall be explored for SFS, such as Singular Value Decomposition (SVD) or Kernel Methods, which overcome this disadvantage.

Further work will also include expanding the original dataset to include other chemistries, such as lithium cobalt oxide (LCO) and nickel cobalt aluminum oxide (NCA).

In addition, using accurate initial values for the optimization algorithm is another important consideration when refitting the weights and the bias from the hidden nodes to the outcome variable, as we proved that using the values of the original NN leads to fast and reliable convergence.

4. Reflections on Applying Transfer Learning to Predict Aging in Lithium-Ion Batteries

In LiB aging, (i) latent features can be identified in data from known battery degradation profiles that would allow capturing patterns in voltage profile or temperature effects, which are associated with capacity fade; (ii) overcomplete representations might ensure the model generalization across different battery types. Moreover, optimal model complexity to avoid overfitting can be avoided by using double descent to explore how overparameterization impacts the generalization error in predicting capacity fade. These reflections lead us to propose the following workflow to enhance the application of transfer learning in predicting aging in LiBs:

- Data preprocessing, which will include collecting and preprocessing aging-related data in battery cycling, including capacity, voltage, temperature, and internal resistance/impedance over time. Dimensionality reduction techniques can be applied to obtain initial insights into the data;
- Representation learning can be used to extract latent features representing degradation mechanisms. A pre-trained model on a large dataset will be then required either on one battery chemistry or a specific usage pattern;
- Transfer learning will be applied for domain adaptation to fine-tune the pre-trained model using smaller datasets from new battery types or different operating conditions;
- The model can be tuned by varying parameters, such as the number of hidden layers, to observe double descent;
- Validation will be required on new or "unseen" battery datasets to assess generalization across domains.

Some of the challenges faced by our theoretical framework include the following:

- Data: Availability of limited high-quality datasets for battery degradation since obtaining these datasets requires significant time and equipment resources. Battery data varies depending on chemistry and operating conditions, and real-world battery data might be noisy and inconsistent;
- Modeling: Several architectures for feature extraction and transfer shall be tested, for which extensive experimentation and domain expertise are required; overparameterized models generalize well theoretically, but they might overfit small dataset unless regularized; generalization across domain is critical to check, as representations learned in the source domain might not generalize well in the target domain; another important feature of battery degradation involves the interaction between variables (in some cases with nonlinear dependencies) that can be challenging to capture;
- Computational resources: Adding high dimensionality to the battery aging phenomenon (e.g., capacity, voltage, current, and impedance) might lead to computationally expensive models in deep architectures. Moreover, training overparameterized models, as well as tuning hyperparameters, can also lead to computationally intensive models;
- Transfer learning: Misalignment in data distribution between source and target domains can negatively impact transfer learning if domain adaptation techniques are not used; fine-tuning the model for a new battery can lead to deviated results, as we can typically expect limited labeled data.

While we recognize that the aging phenomenon in LiBs is complex that the battery SOH cannot be limited to assessing capacity fade alone—requiring instead the aggregation and study of the interaction of battery chemistry, electrolyte, operating conditions, and other aging indicators such as internal resistance/impedance and voltage—we believe that our transfer learning exercise balances the current picture in the battery testing and modeling universe with the emerging possibility of applying transfer learning for limited target datasets. Another important consideration in this regard for future work and for generating tailored aging data for transfer learning is to consistently generate data among battery chemistries. These data should include an operational envelope that allows capturing aging to extrapolate to real-life conditions while recording several aging-related indicators per experiment. These features are currently not included in all datasets, presumably due to the extensive time and equipment resources required for cycling battery cells. In this regard, we strongly believe that overparameterized models can be useful for feature extraction and generalization. However, the current datasets might be limited in offering sufficient variation, such as for user patterns and operating conditions to capture different degradation mechanisms and battery chemistry. With limited datasets and fewer features, we might encounter the risk of overfitting and even overrepresenting patterns that are not fully aligned with physical degradation, as we believe that capacity fade alone does not fully capture all degradation mechanisms.

We finally recommend some strategies to overcome the challenges previously described, including synthetic data generation, integrating domain knowledge into models through physics-informed machine learning, applying domain adaptation techniques for transfer learning, and using regularization to prevent overfitting in overparameterized models.

5. Conclusions

In this work, we proposed an adaptive transfer learning (TL) approach to predict the aging of lithium-ion batteries (LiBs) using capacity fade as the indicator of the battery state of health (SOH). The source data used for TL were selected by combining feature and stress factor similarities and time series similarities compared to the target data, aiming at increasing the prediction accuracy of the TL process, as features and patterns learned from the source data were relevant for the target data.

Similarity-based data selection improves the effectiveness of TL in predicting capacity fade with limited data. Thus, in the example used to illustrate the implementation of the proposed TL approach, the similarity contribution from features and stress factors ($\alpha = 0.7$) led to an error reduction of -4.7% for a threshold of $\beta = 5$. This finding emphasizes the importance of selecting representative and balanced data in both feature/stress factors and time domains.

The size of the clean dataset obtained from the original dataset also plays a critical role in the effectiveness of the TL process, but only in combination with the trade-off of α and β, so that the data are sufficient but representative of TL. The error reduction when applying our TL approach lies between -0.4% and -8.3% for multiple computational experiments, further confirming its robustness. The main takeaways of these results are the following: (i) features/stress factors similarities shall be emphasized over time series similarities to improve TL performance, (ii) moderate β values ensure a tradeoff between data diversity and representation, and (iii) large and diverse clean datasets typically correlate with better TL performance metrics.

Further exploration of alternative similarity algorithms, such as Singular Value Decomposition or Kernel Methods, could provide a more efficient means of comparing feature sets with different dimensions, as the Frobenius norm can only be used with same-size matrices.

Key reflections from our findings led us to propose a workflow for transfer learning in predicting LiB aging, which includes recommendations on data preprocessing, representation learning, transfer learning, model tuning, and validation. Challenges for our framework implementation include limited quality datasets, data variability, risk of overfitting small datasets, models that might not effectively capture the interaction between variables, intensive computation resources required for high dimensionality and overparameterized models, and misalignment in data distribution between source and target domains. The corresponding recommendations to overcome these challenges include generating synthetic data, integrating domain knowledge through physics-informed machine learning, applying domain adaptation techniques, and using regularization to avoid overfitting in overparameterized models.

This study has laid the foundation for future work in data-driven machine-learning battery aging modeling, as our adaptive transfer learning approach could offer a pragmatic solution to predict SOH with limited data availability. Despite promising results, challenges remain, including finding a trade-off for α and β, ensuring data representativeness and sufficiency, balancing data similarity and diversity, generalizing our approach for other cell cathode chemistries such as lithium cobalt oxide (LCO) and nickel cobalt aluminum oxide (NCA), and including other aging indicators to gain a better insight into the battery SOH.

Author Contributions: Conceptualization, D.G.; methodology, D.G. and M.S.; software, D.G. and M.S.; validation D.G.; formal analysis, D.G.; investigation, D.G. and M.S.; resources, C.H.A. data curation, M.S.; writing—original draft preparation, D.G.; writing—review and editing, C.H.A.; visualization, D.G.; supervision, C.H.A.; project administration, C.H.A.; funding acquisition, C.H.A. All authors have read and agreed to the published version of the manuscript.

Funding: This work was supported by the Natural Sciences and Engineering Research Council of Canada (NSERC), eCAMION/JULE Inc., and Ford Motor Company of Canada Ltd.

Data Availability Statement: Data are available upon request.

Conflicts of Interest: The authors declare no conflicts of interest. The funders had no role in the design of the study; in the collection, analyses, or interpretation of data; in the writing of the manuscript; or in the decision to publish the results. The authors declare that this study received funding from NSERC, and eCAMION/JULE Inc. The funders were not involved in the study design, collection, analysis, interpretation of data, the writing of this article or the decision to submit it for publication.

Abbreviations

The following abbreviations are used in this manuscript:

BGFS	Broyden-Fletcher-Goldfarb-Shann
C-rate	Charge/discharge rates
CD	Clean dataset
DOD	Depth-of-discharge
DTW	Dynamic Time Warping
ECM	Equivalent circuit model
EDA	Exploratory data analysis
EIS	Electrochemical Impedance Spectroscopy
EV	Electric vehicle
LP	Lithium plating
LiB	Lithium-ion Battery
NH	Number of hidden nodes
NN	Neural network

OD	Original dataset
RMSE	Root mean squared error
RUL	Remaining Useful Life
SEI	Solid electrolyte interface
SFS	Features/stress factor similarity
SOC	State-of-charge
SOH	State-of-health
SSE	Sum of squared error
STS	Time series similarity
TDS	Total data similarity
TL	Transfer learning

Appendix A

Table A1. Detailed information on the aging data compiled from the literature.

Experiment	Nominal Capacity Ah	Chemistry and Format	Description	Ref.
1	28	111 Prismatic	T = 40 °C, SOC = 50%, DOD = 100%, C-rate: 1/1	[19]
2 to 4	3	622 Pouch	T = 25, 35, 45 °C, SOC = 50%, DOD = 100%, C-rate: 1/1	[20]
5 to 7	0.4	622 Pouch	T = 30 °C, SOC = 50%, DOD = 100%, C-rate: 1/1, 4/1, 6/1	[21]
8	1	622 Pouch	T = 45 °C, SOC = 50%, DOD = 100%, C-rate: 0.5/0.5	[22]
9 to 11	31	433 Pouch	T = 5, 15, 45 °C, SOC = 50%, DOD = 100%, C-rate: 1/1	[23]
12 to 16	64	532 Pouch	T = 5, 15, 25, 35, 45 °C, SOC = 50%, DOD = 100%, C-rate: 0.75/0.75	[23]
17, 18	0.6	622 Pouch	T = 0, 25 °C, SOC = 50%, DOD = 100%, C-rate: 0.5/0.5, 1/1	[24]
19	0.088	622 Pouch	T = 25 °C, SOC = 50%, DOD = 100%, C-rate: 2/3	[25]
20	37	111 Pouch	T = 25 °C, SOC = 92.5%, DOD = 7%, C-rate: 1.26/4	[26]
21	0.81	622 Pouch	T = 45 °C, SOC = 50%, DOD = 100%, C-rate: 1/1	[27]

Table A1. *Cont.*

Experiment	Nominal Capacity Ah	Chemistry and Format	Description	Ref.
22	0.8	622 Pouch	T = 45 °C, SOC = 50%, DOD = 100%, C-rate: 1/0.5	[28]
23	0.52	622 Pouch	T = 30 °C, SOC = 50%, DOD = 100%, C-rate: 4/1	[29]
24	3.3	622 Pouch	T = 25 °C, SOC = 50%, DOD = 100%, C-rate: 1/2	[30]
25	7.8	111 Pouch	T = 20 °C, SOC = 50%, DOD = 100%, C-rate: 1.28/1.28	[31]
26, 27	34	111 Prismatic	T = 10, 25 °C, SOC = 50%, DOD = 100%, C-rate: 1/1	[32]
28 to 30	3	811 Cylindrical	T = 15, 25, 35 °C, SOC = 50%, DOD = 100%, C-rate: 0.5/0.5, 1/1	[33]
31, 32	2.2	532 Cylindrical	T = 20, 45 °C, SOC = 50%, DOD = 100%, C-rate: 1/1	[34]
33 to 38	3	811 Cylindrical	T = 15, 25, 35 °C, SOC = 50%, DOD = 100%, C-rate: 0.5/0.5, 0.5/1, 0.5/2, 0.5/3	[35]
39 to 42	64	111 Pouch	T = 10, 30, 45 °C, SOC = 50%, DOD = 100%, C-rate: 0.3/0.9, 1/1, 2/1, 2/0.5	[36]
43 to 49	20	442 Pouch	T = 10, 25, 45 °C, SOC = 50%, DOD = 20, 50, 90%, C-rate: 0.5/1, 0.5/2	[37]
50	2.6	532 Cylindrical	T = 22 °C, SOC = 50%, DOD = 100%, C-rate: 0.5/0.5	[38]
51 to 53	20	442 Pouch	T = 25 °C, SOC = 50, 60%, DOD = 80, 100%, C-rate: 0.33/0.33, 0.33/1, 1/1	[39]
54, 55	5	622 Pouch	T = 20, 45 °C, SOC = 50%, DOD = 100%, C-rate: 1/1	[40]
56 to 61	25, 28, 37	111 Prismatic	T = 35 °C, SOC = 50%, DOD = 60%, C-rate: 1/1, 3/1	[41]

Table A1. *Cont.*

Experiment	Nominal Capacity Ah	Chemistry and Format	Description	Ref.
62	58.9	622 Pouch	T = −10, −20, −25 °C, SOC = 50%, DOD = 100%, C-rate: 0.25/0.25	[42]
63 to 83	20	442 Pouch	T = 25, 35 °C, SOC = 35, 50, 65%, DOD = 20, 65, 80, 100%, C-rate: 0.33/1, 0.33/2, 0.5/1, 1/1, 2/2	[43]
84 to 87	25	111 Prismatic	T = 35 °C, SOC = 50%, DOD = 60%, C-rate: 1/1, 2/1, 3/1, 4/1	[44]
88 to 91	63	111 Pouch	T = 25, 40 °C, SOC = 50%, DOD = 100%, C-rate: 1/1, 1/3, 1/2, 3/1,	[45]
92 to 98	10	111 Pouch	T = 5, 25, 40, 60 °C, SOC = 50, 75, 95%, DOD = 10, 50, 100%, C-rate: 1/1	[46]
99	2.2	532 Cylindrical	T = 35 °C, SOC = 50%, DOD = 100%, C-rate: 1/2	[47]
100	20	442 Pouch	T = 35 °C, SOC = 50%, DOD = 80%, C-rate: 1/1	[48]

References

1. Galatro, D.; Al-Zareer, M.; Da Silva, C.; Romero, D.A.; Amon, C.H. Thermal Behavior of Lithium-Ion Batteries: Aging, Heat Generation, Thermal Management and Failure. *Front. Heat. Mass. Transf.* **2020**, *14*, 1–18. [CrossRef]
2. Energy Batteries Loss of Electrolyte in Batteries: Causes, Effects, and Mitigation Strategies. Available online: https://www.energy-batteries.com/loss-of-electrolyte-in-batteries-causes-effects-and-mitigation-strategies/ (accessed on 6 January 2025).
3. Chen, B.R.; Police, Y.R.; Li, M.; Chinnam, P.R.; Tanim, T.R.; Dufek, E.J. A Mathematical Approach to Survey Electrochemical Impedance Spectroscopy for Aging in Lithium-Ion Batteries. *Front. Energy Res.* **2023**, *11*, 1132876. [CrossRef]
4. Nikolian, A.; Jaguemont, J.; de Hoog, J.; Goutam, S.; Omar, N.; Van Den Bossche, P.; Van Mierlo, J. Complete Cell-Level Lithium-Ion Electrical ECM Model for Different Chemistries (NMC, LFP, LTO) and Temperatures (−5 °C to 45 °C)—Optimized Modelling Techniques. *Int. J. Electr. Power Energy Syst.* **2018**, *98*, 133–146. [CrossRef]
5. Galatro, D.; Silva, C.D.; Romero, D.A.; Trescases, O.; Amon, C.H. Challenges in Data-Based Degradation Models for Lithium-Ion Batteries. *Int. J. Energy Res.* **2020**, *44*, 3954–3975. [CrossRef]
6. Galatro, D.; Da Silva, C.; Romero, D.A.; Gong, Z.; Trescases, O.; Amon, C.H. Battery Health Diagnosis Approach Integrating Physics-Based Modeling with Electrochemical Impedance Spectroscopy. *Energy Technol.* **2022**, *10*, 2100942. [CrossRef]
7. *APEC 2020: Thirty-Fifth Annual IEEE Applied Power Electronics Conference and Exposition: 15–19 March 2020, New Orleans, Louisiana*; IEEE: New York, NY, USA, 2020; ISBN 9781728148298.
8. Jia, X.; Zhang, C.; Wang, L.Y.; Zhang, L.; Zhou, X. Early Diagnosis of Accelerated Aging for Lithium-Ion Batteries with an Integrated Framework of Aging Mechanisms and Data-Driven Methods. *IEEE Trans. Transp. Electrif.* **2022**, *8*, 4722–4742. [CrossRef]
9. Li, X.; Ju, L.; Geng, G.; Jiang, Q. Data-Driven State-of-Health Estimation for Lithium-Ion Battery Based on Aging Features. *Energy* **2023**, *274*, 127378. [CrossRef]
10. Zhang, C.; Du, J.; Li, S.; Zhang, L.; Zhang, W. Cross-Domain Machine Transfer Learning for Capacity Aging Trajectory Prediction of Lithium-Ion Batteries. *J. Power Sources* **2024**, *624*, 235534. [CrossRef]
11. Galatro, D.; Machavolu, M.; Navas, G. Transfer Learning Strategies for Neural Networks: A Case Study in Amine Gas Treating Units. *Results Eng.* **2024**, *24*, 103027. [CrossRef]

12. Yang, Q.; Zhang, Y.; Dai, W.; Pan, S.J. *Transfer Learning*; Cambridge University Press: Cambridge, UK, 2020; ISBN 9781139061773.
13. Adlam, B.; Pennington, J. The Neural Tangent Kernel in High Dimensions: Triple Descent and a Multi-Scale Theory of Generalization. *arXiv* **2020**, arXiv:2008.06786.
14. Bengio, Y. *Deep Learning of Representations for Unsupervised and Transfer Learning*; JMLR.org: Washington, DC, USA, 2012; Volume 27.
15. Li, Z.; Bai, F.; Zuo, H.; Zhang, Y. Remaining Useful Life Prediction for Lithium-Ion Batteries Based on Iterative Transfer Learning and Mogrifier LSTM. *Batteries* **2023**, *9*, 448. [CrossRef]
16. Chen, C.; Wei, J.; Li, Z. Remaining Useful Life Prediction for Lithium-Ion Batteries Based on a Hybrid Deep Learning Model. *Processes* **2023**, *11*, 2333. [CrossRef]
17. Chen, X.; Liu, Z.; Sheng, H.; Wu, K.; Mi, J.; Li, Q. Transfer Learning Based Remaining Useful Life Prediction of Lithium-Ion Battery Considering Capacity Regeneration Phenomenon. *J. Energy Storage* **2024**, *76*, 109798. [CrossRef]
18. Koutra, D.; Plant, C.; Gomez Rodriguez, M.; Baralis, E.; Bonchi, F. (Eds.) *Machine Learning and Knowledge Discovery in Databases: Research Track*; Lecture Notes in Computer Science; Springer Nature Switzerland: Cham, Switzerland, 2023; Volume 14173, ISBN 978-3-031-43423-5.
19. Bessman, A.; Soares, R.; Wallmark, O.; Svens, P.; Lindbergh, G. Aging Effects of AC Harmonics on Lithium-Ion Cells. *J. Energy Storage* **2019**, *21*, 741–749. [CrossRef]
20. Lee, Y.J.; Choi, H.Y.; Ha, C.W.; Yu, J.H.; Hwang, M.J.; Doh, C.H.; Choi, J.H. Cycle Life Modeling and the Capacity Fading Mechanisms in a Graphite/LiNi0.6Co0.2Mn0.2O2 Cell. *J. Appl. Electrochem.* **2015**, *45*, 419–426. [CrossRef]
21. Wu, X.; Bai, Y.; Li, Z.; Liu, J.; Zhao, K.; Du, Z. Effects of Charging Rates on LiNi0.6Mn0.2Co0.2O2 (NMC622)/Graphite Li-Ion Cells. *J. Energy Chem.* **2021**, *56*, 121–126. [CrossRef]
22. Xu, D.; Kang, Y.; Wang, J.; Hu, S.; Shi, Q.; Lu, Z.; He, D.; Zhao, Y.; Qian, Y.; Lou, H.; et al. Exploring Synergetic Effects of Vinylene Carbonate and 1,3-Propane Sultone on LiNi0.6Mn0.2Co0.2O2/Graphite Cells with Excellent High-Temperature Performance. *J. Power Sources* **2019**, *437*, 226929. [CrossRef]
23. Spitthoff, L.; Vie, P.J.S.; Wahl, M.S.; Wind, J.; Burheim, O.S. Incremental Capacity Analysis (DQ/DV) as a Tool for Analysing the Effect of Ambient Temperature and Mechanical Clamping on Degradation. *J. Electroanal. Chem.* **2023**, *944*, 117627. [CrossRef]
24. Lin, Y.; Xu, M.; Wu, S.; Tian, Y.; Cao, Z.; Xing, L.; Li, W. Insight into the Mechanism of Improved Interfacial Properties between Electrodes and Electrolyte in the Graphite/LiNi0.6Mn0.2Co0.2O2 Cell via Incorporation of 4-Propyl-[1,3,2]Dioxathiolane-2,2-Dioxide (PDTD). *ACS Appl. Mater. Interfaces* **2018**, *10*, 16400–16409. [CrossRef] [PubMed]
25. Stockhausen, R.; Gehrlein, L.; Müller, M.; Bergfeldt, T.; Hofmann, A.; Müller, F.J.; Maibach, J.; Ehrenberg, H.; Smith, A. Investigating the Dominant Decomposition Mechanisms in Lithium-Ion Battery Cells Responsible for Capacity Loss in Different Stages of Electrochemical Aging. *J. Power Sources* **2022**, *543*, 231842. [CrossRef]
26. Sieg, J.; Storch, M.; Fath, J.; Nuhic, A.; Bandlow, J.; Spier, B.; Sauer, D.U. Local Degradation and Differential Voltage Analysis of Aged Lithium-Ion Pouch Cells. *J. Energy Storage* **2020**, *30*, 101582. [CrossRef]
27. Gao, J.; Qin, Z.; Zhao, G.; Liu, Y.; Zhang, W.; Yao, H.; Zheng, Y.; Lin, Y.; Huang, Z.; Li, J. Modulating NCM622 Electrode to Efficiently Boost the Lithium Storage and Thermal Safety of Its Full Batteries. *Energy Storage Mater.* **2024**, *67*, 103332. [CrossRef]
28. Aupperle, F.; Eshetu, G.G.; Eberman, K.W.; Xioa, A.; Bridel, J.S.; Figgemeier, E. Realizing a High-Performance LiNi0.6Mn0.2Co0.2O2/Silicon-Graphite Full Lithium Ion Battery Cell: Via a Designer Electrolyte Additive. *J. Mater. Chem. A Mater.* **2020**, *8*, 19573–19587. [CrossRef]
29. Wu, X.; Ma, L.; Liu, J.; Zhao, K.; Wood, D.L.; Du, Z. Understanding the Effect of Salt Concentrations on Fast Charging Performance of Li-Ion Cells. *J. Power Sources* **2022**, *545*, 231863. [CrossRef]
30. Leng, Y.; Ge, S.; Marple, D.; Yang, X.-G.; Bauer, C.; Lamp, P.; Wang, C.-Y. Electrochemical Cycle-Life Characterization of High Energy Lithium-Ion Cells with Thick $Li(Ni_{0.6}Mn_{0.2}Co_{0.2})O_2$ and Graphite Electrodes. *J. Electrochem. Soc.* **2017**, *164*, A1037–A1049. [CrossRef]
31. Heins, T.P.; Schlüter, N.; Ernst, S.T.; Schröder, U. On the Interpretation of Impedance Spectra of Large-Format Lithium-Ion Batteries and Its Application in Aging Studies. *Energy Technol.* **2020**, *8*, 1900279. [CrossRef]
32. Schmitt, J.; Kraft, B.; Schmidt, J.P.; Meir, B.; Elian, K.; Ensling, D.; Keser, G.; Jossen, A. Measurement of Gas Pressure inside Large-Format Prismatic Lithium-Ion Cells during Operation and Cycle Aging. *J. Power Sources* **2020**, *478*, 228661. [CrossRef]
33. Wittman, R.; Dubarry, M.; Ivanov, S.; Juba, B.W.; Romàn-Kustas, J.; Fresquez, A.; Langendorf, J.; Grant, R.; Taggart, G.; Chalamala, B.; et al. Characterization of Cycle-Aged Commercial NMC and NCA Lithium-Ion Cells: I. Temperature-Dependent Degradation. *J. Electrochem. Soc.* **2023**, *170*, 120538. [CrossRef]
34. Friesen, A.; Mönnighoff, X.; Börner, M.; Haetge, J.; Schappacher, F.M.; Winter, M. Influence of Temperature on the Aging Behavior of 18650-Type Lithium Ion Cells: A Comprehensive Approach Combining Electrochemical Characterization and Post-Mortem Analysis. *J Power Sources* **2017**, *342*, 88–97. [CrossRef]

35. Preger, Y.; Barkholtz, H.M.; Fresquez, A.; Campbell, D.L.; Juba, B.W.; Romàn-Kustas, J.; Ferreira, S.R.; Chalamala, B. Degradation of Commercial Lithium-Ion Cells as a Function of Chemistry and Cycling Conditions. *J. Electrochem. Soc.* **2020**, *167*, 120532. [CrossRef]
36. Gasper, P.; Sunderlin, N.; Dunlap, N.; Walker, P.; Finegan, D.P.; Smith, K.; Thakkar, F. Lithium Loss, Resistance Growth, Electrode Expansion, Gas Evolution, and Li Plating: Analyzing Performance and Failure of Commercial Large-Format NMC-Gr Lithium-Ion Pouch Cells. *J. Power Sources* **2024**, *604*, 234494. [CrossRef]
37. Hosen, M.S.; Karimi, D.; Kalogiannis, T.; Pirooz, A.; Jaguemont, J.; Berecibar, M.; Van Mierlo, J. Electro-Aging Model Development of Nickel-Manganese-Cobalt Lithium-Ion Technology Validated with Light and Heavy-Duty Real-Life Profiles. *J. Energy Storage* **2020**, *28*, 101265. [CrossRef]
38. Weisenberger, C.; Meir, B.; Röhler, S.; Harrison, D.K.; Knoblauch, V. A Post-Mortem Study of Commercial 18650 Lithium-Ion Cells with LiNi0.5Co0.2Mn0.3O2//Graphite Chemistry after Prolonged Cycling (> 7000 Cycles) with Low C-Rates. *Electrochim Acta* **2021**, *379*, 138145. [CrossRef]
39. Shafiei Sabet, P.; Warnecke, A.J.; Meier, F.; Witzenhausen, H.; Martinez-Laserna, E.; Sauer, D.U. Non-Invasive yet Separate Investigation of Anode/Cathode Degradation of Lithium-Ion Batteries (Nickel–Cobalt–Manganese vs. Graphite) Due to Accelerated Aging. *J. Power Sources* **2020**, *449*, 227369. [CrossRef]
40. Münster, P.; Diehl, M.; Frerichs, J.E.; Börner, M.; Hansen, M.R.; Winter, M.; Niehoff, P. Effect of Li Plating during Formation of Lithium Ion Batteries on Their Cycling Performance and Thermal Safety. *J. Power Sources* **2021**, *484*, 229306. [CrossRef]
41. Svens, P.; Smith, A.J.; Groot, J.; Lacey, M.J.; Lindbergh, G.; Lindstrom, R.W. Evaluating Performance and Cycle Life Improvements in the Latest Generations of Prismatic Lithium-Ion Batteries. *IEEE Trans. Transp. Electrif.* **2022**, *8*, 3696–3706. [CrossRef]
42. Zhao, X.; Yin, Y.; Hu, Y.; Choe, S.Y. Electrochemical-Thermal Modeling of Lithium Plating/Stripping of Li(Ni0.6Mn0.2Co0.2)O2/Carbon Lithium-Ion Batteries at Subzero Ambient Temperatures. *J. Power Sources* **2019**, *418*, 61–73. [CrossRef]
43. Warnecke, A.J. Degradation Mechanisms in NMC Batteries *Aachener Beiträge Des ISEA*. Volume 105. Available online: https://publications.rwth-aachen.de/record/708098/files/708098.pdf (accessed on 6 January 2025).
44. Mussa, A.S.; Liivat, A.; Marzano, F.; Klett, M.; Philippe, B.; Tengstedt, C.; Lindbergh, G.; Edström, K.; Lindström, R.W.; Svens, P. Fast-Charging Effects on Ageing for Energy-Optimized Automotive LiNi1/3Mn1/3Co1/3O2/Graphite Prismatic Lithium-Ion Cells. *J. Power Sources* **2019**, *422*, 175–184. [CrossRef]
45. Arunachala, R.; Makinejad, K.; Athlekar, S.; Jossen, A.; Garche, J. Cycle Life Characterisation of Large Format Lithium-Ion Cells. In Proceedings of the 2013 World Electric Vehicle Symposium and Exhibition (EVS27), Barcelona, Spain, 17–20 November 2013.
46. Käbitz, S.; Gerschler, J.B.; Ecker, M.; Yurdagel, Y.; Emmermacher, B.; André, D.; Mitsch, T.; Sauer, D.U. Cycle and Calendar Life Study of a Graphite | LiNi1/3Mn 1/3Co1/3O2 Li-Ion High Energy System. Part A: Full Cell Characterization. *J. Power Sources* **2013**, *239*, 572–583. [CrossRef]
47. Guo, J.; Jin, S.; Sui, X.; Huang, X.; Xu, Y.; Li, Y.; Kristensen, P.K.; Wang, D.; Pedersen, K.; Gurevich, L.; et al. Unravelling and Quantifying the Aging Processes of Commercial Li(Ni0.5Co0.2Mn0.3)O2/Graphite Lithium-Ion Batteries under Constant Current Cycling. *J. Mater. Chem. A Mater.* **2022**, *11*, 41–52. [CrossRef]
48. Capron, O.; Jaguemont, J.; Gopalakrishnan, R.; Van den Bossche, P.; Omar, N.; Van Mierlo, J. Impact of the Temperature in the Evaluation of Battery Performances during Long-Term Cycling-Characterisation and Modelling. *Appl. Sci.* **2018**, *8*, 1364. [CrossRef]
49. Galatro, D.; Romero, D.A.; Freitez, J.A.; Da Silva, C.; Trescases, O.; Amon, C.H. Modeling Degradation of Lithium-Ion Batteries Considering Cell-to-Cell Variations. *J. Energy Storage* **2021**, *44*, 103478. [CrossRef]
50. Galatro, D.; Romero, D.A.; Da Silva, C.; Trescases, O.; Amon, C.H. Impact of Cell Spreading on Second-Life of Lithium-Ion Batteries. *Can. J. Chem. Eng.* **2022**, *101*, 1114–1122. [CrossRef]